



Ni₃(C₃N₃S₃)₂ coordination polymer as a novel broad spectrum-driven photocatalyst for water splitting into hydrogen



Feng Guo^{a,b}, Weilong Shi^{a,c}, Sijie Guo^a, Weisheng Guan^b, Yanhong Liu^{d,*}, Hui Huang^{a,*}, Yang Liu^{a,*}, Zhenhui Kang^{a,*}

^a Jiangsu Key Laboratory for Carbon-Based Functional Materials & Devices, Institute of Functional Nano & Soft Materials (FUNSOM), Soochow University, 199 Ren'ai Road, Suzhou, 215123, Jiangsu, PR China

^b Key Laboratory of Subsurface Hydrology and Ecological Effects in Arid Region, Ministry of Education, School of Environmental Science and Engineering, Chang'an University, Xi'an, 710064, PR China

^c School of Physics, Huazhong University of Science and Technology, Wuhan, 430074, PR China

^d Institute of Green Chemistry and Chemical Technology, Jiangsu University, Zhenjiang, 212013, PR China

ARTICLE INFO

Article history:

Received 2 February 2017

Received in revised form 10 March 2017

Accepted 24 March 2017

Available online 27 March 2017

Keywords:

Coordination polymer

Photocatalyst

Ni₃(C₃N₃S₃)₂

Water splitting

Board spectrum-driven

ABSTRACT

Sparked by the increasing energy crisis, much research has been focused on seeking board spectrum-driven photocatalysts for water splitting. Herein, the Ni₃(C₃N₃S₃)₂ coordination polymer was firstly synthesized by a simple wet-chemical method, as a novel board spectrum-driven photocatalyst for water splitting. The as-prepared Ni₃(C₃N₃S₃)₂ exhibited excellent photocatalytic H₂-producing activity from the half-reaction of water splitting without the help of any sacrificial agents or cocatalysts, and the amounts of H₂ production are 65.3, 53.9 and 16.3 μmol corresponding to UV ($\lambda < 400$ nm), visible ($400 \leq \lambda \leq 760$ nm) and near-infrared ($\lambda > 760$ nm) irradiation after 24 h, respectively. Another valuable finding is that after adding triethanolamine as a sacrificial donor, the average H₂ evolution efficiencies on Ni₃(C₃N₃S₃)₂ were efficaciously increased by around 2-fold with the H₂ production value of 112.6, 93.3 and 30.1 μmol for 24 h under the UV light, visible light and near-infrared light exposure, respectively. More importantly, the stability of Ni₃(C₃N₃S₃)₂ was effectively improved by means of triethanolamine. The results facilitate the increasing attention of narrow band gap non-noble metal coordination polymers treated as board spectrum-driven photocatalysts for expanding the utilization of solar light.

© 2017 Elsevier B.V. All rights reserved.

1. Introduction

Sparked by the increasing energy crisis, widespread attention has been focusing on the development and utilization of renewable energy to supersede the limited fossil fuel [1]. Among all the renewable energy, solar energy is not only the most important basic energy, but also extensively utilized by human beings. Over the last decade, photocatalysis has caused considerable interest for environmental protection and energy production utilizing inexhaustible solar energy since the first reported by Fujishima and Honda in 1972 [2]. Up to present, UV- and visible (Vis) light-driven photocatalytic systems have aroused worldwide research, and numerous photocatalysts with excellent photocatalytic activities have been found, such as TiO₂ [3], ZnO [4], SnO₂ [5] in the UV

range (ca. 4% of solar spectrum), InVO₄ [6], BiVO₄ [7], CdS [8] in the range of visible light (ca. 44% of solar spectrum). It is worthwhile mentioning that the near-infrared (NIR) light of more than 50% in the solar spectrum has remained unutilized in photocatalysis research [9].

In the last three decades, pioneering works of NIR light-active photocatalysts have been paid close attention to the up-conversion luminescence of rare earth materials (e.g. Yb:Tm:YF₃/TiO₂ [10] and BiErWO₆ [11]) that can convert NIR light into Vis and UV light for exhibiting excellent NIR photocatalytic activity. Nevertheless, the efficient utilization of up-conversion photocatalyst was limited because a 980 nm laser had to be applied for an overall low conversion [12]. Another new mechanism was proposed to construct a nanostructure with surface plasmon resonance (SPR) effect for improving the utilization of light. For instance, Pt-tipped Au nanorods-based photocatalysts shows outstanding H₂ production activity under Vis and NIR light irradiation [13]. The hot electrons can be excited due to the SPR effect of Au nanorods and rapidly transferred to the Pt tip. However, the high cost of precious metals

* Corresponding authors.

E-mail addresses: liuyh@ujs.edu.cn (Y. Liu), hhuang0618@suda.edu.cn (H. Huang), yangl@suda.edu.cn (Y. Liu), zhkang@suda.edu.cn (Z. Kang).

will hinder the practical application of such photocatalyst. In addition to the up-conversion materials and SPR-based photocatalyst, many single-component valuable photocatalysts with Vis-NIR or NIR photocatalytic activity were developed, such as Bi_2WO_6 [14] and WS_2 [15]. Unfortunately, the synthetic methods of above NIR-driven photocatalysts were carried out with hydrothermal route at high pressure or high sintering temperature, which increase loss of resources in the production process. Therefore, it is still a significant challenge to search for UV-vis-near infrared (UV-vis-NIR) board spectrum-driven photocatalysts with facile synthesis and price moderate.

In this study, a novel $\text{C}_3\text{N}_3\text{S}_3$ -based noble metal-free coordination polymer, $\text{Ni}_3(\text{C}_3\text{N}_3\text{S}_3)_2$, was firstly synthesized via a facile wet-chemical route at room temperature. Specifically, the as-prepared $\text{Ni}_3(\text{C}_3\text{N}_3\text{S}_3)_2$ possessed UV-vis-NIR broad spectrum absorption and can be employed as a board spectrum-driven photocatalyst for water splitting into hydrogen. The $\text{Ni}_3(\text{C}_3\text{N}_3\text{S}_3)_2$ exhibited excellent photocatalytic H_2 -producing activity from the half-reaction of water splitting without the help of any sacrificial agents or cocatalysts, and the amounts of H_2 production are 65.3, 53.9 and 16.3 μmol corresponding to UV ($\lambda < 400 \text{ nm}$), Vis ($400 \leq \lambda \leq 760 \text{ nm}$) and NIR ($\lambda > 760 \text{ nm}$) irradiation after 24 h, respectively. Another valuable finding is that after adding triethanolamine as a sacrificial donor, the average H_2 evolution efficiencies on $\text{Ni}_3(\text{C}_3\text{N}_3\text{S}_3)_2$ were efficaciously increased by around 2-fold with the H_2 production value of 112.6, 93.3 and 30.1 μmol for 24 h under the UV, Vis and NIR light exposure, respectively. More importantly, the photostability of $\text{Ni}_3(\text{C}_3\text{N}_3\text{S}_3)_2$ was effectively improved by means of triethanolamine. Moreover, a possible photocatalytic mechanism of the $\text{Ni}_3(\text{C}_3\text{N}_3\text{S}_3)_2$ photocatalyst was also proposed.

2. Experimental section

2.1. Materials

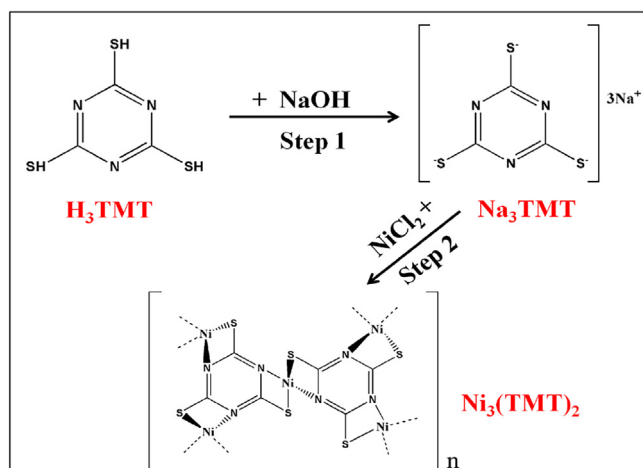
$\text{NiCl}_2 \cdot 6\text{H}_2\text{O}$ and NaOH were purchased from Sinopharm chemical reagent Co., Ltd (Shanghai, China) and trithiocyanuric acid (H_3TMT) was supplied by Xiya chemical reagent Co., Ltd (Chengdu, China).

2.2. Preparation of $\text{Ni}_3(\text{TMT})_2$

Similar to previously reported method [16], the wet-chemical synthesis at room temperature was applied to prepared the $\text{Ni}_3(\text{TMT})_2$. Accordingly, 0.24 g NaOH and H_3TMT were dissolved in 100 mL demineralized water to form a transparent solution (Na_3TMT aqueous solution). Simultaneously, 0.714 g $\text{NiCl}_2 \cdot 6\text{H}_2\text{O}$ was added in 100 mL demineralized water (NiCl_2 aqueous solution). Afterwards, the NiCl_2 aqueous solution was dropped slowly into Na_3TMT aqueous solution and aged for 24 h mildly stirring. The resulting products were washed by demineralized water, and finally dried at 70 °C in vacuum oven.

2.3. Characterization

X-ray photoelectron spectroscopy (XPS) analyses of sample were implemented on an ESCALABMK II X-ray photoelectron spectrometer. The Fourier Transform Infrared (FT-IR) spectrum of samples was obtained by a Nicolet-360 spectrometer. X-ray powder diffraction (XRD) patterns of $\text{Ni}_3(\text{TMT})_2$ were carried out with an X'Pert-ProMPD (Holand) D/max- γ AX-ray diffract meter. Scanning electron microscopy (SEM) images and energy dispersive X-ray analysis spectroscopy (EDS) were collected with an FEI-quanta 200 scanning electron microscope. Transmission electron microscopy (TEM) and high-resolution TEM (HRTEM) images



Scheme 1. The formation route of $\text{Ni}_3(\text{TMT})_2$ photocatalyst.

were taken on an FEI-Tecnai F20 (200 kV), respectively. UV-vis-NIR diffuse reflectance spectrum was recorded on a Lambda 750 (Perkin-Elmer) spectrophotometer with the range of 200–2500 nm. Electrochemical measurements were conducted on a CHI 660B workstation with a standard three-electrode cell. The Pt wire, a calomel electrode, and the samples were used as the counter electrode, the reference electrode, and the working electrode, respectively. The synthesis of working electrodes was in line with the previous literature [17]. For photocurrent response and electrochemical impedance spectroscopy (EIS) measurements, a 300 W Xe lamp with different wavelength filters served as Vis or NIR light source and a Na_2SO_4 (0.5 M) aqueous solution was used as the electrolyte. EIS was recorded by applying an AC voltage of 5 mV amplitude in the frequency range of 10^5 – 10^{-2} Hz with the open circuit voltage. Mott-Schottky (MS) plots are also obtained in Na_2SO_4 (0.5 M) aqueous solution with the frequency of 5000 Hz.

2.4. Photocatalytic activity test

The photocatalytic reactions were conducted in a Pyrex glass photoreactor with a flat window at the top for illumination connected to a closed gas-circulation system. The 300 mg catalyst powder was dispersed in 100 mL ultrapure water, and then the system was completely degassed to remove air through a vacuuming procedure. Under ambient conditions and constant stirring, the AM 1.5G solar simulator (MICROSOLAR 300, Beijing Perfectlight Co. Ltd, China) was applied as the UV light, visible light and near-infrared light source, under assistance of filters to ensure the light $< 400 \text{ nm}$ as UV source, light of 400–760 nm as Vis source as well as the light $> 760 \text{ nm}$ as NIR source. For evolved gas detection, an online GC-7900 gas chromatograph set up with a thermal conductivity detector (TCD) and 5 Å molecular sieve columns was employed. The oven, injection port and detector temperatures of gas chromatograph were held at 80, 100, and 120 °C, respectively. Ar was used as carrier gas with the flow rate of 30 mL/min. To check the reproducibility and stability of catalysts, the suspension after reaction was centrifuged and reused for repeated tests.

3. Results and discussion

In this study, we synthesized $\text{Ni}_3(\text{C}_3\text{N}_3\text{S}_3)_2$ via a facile wet-chemical route at room temperature. As described in Scheme 1, two steps were given. One step was that the precursor trithiocyanuric acid ($\text{H}_3\text{C}_3\text{N}_3\text{S}_3$) combined with NaOH to form 1,3,5-Triazine-2,4,6-triol trisodium salt solution ($\text{Na}_3\text{C}_3\text{N}_3\text{S}_3$). Then, $\text{Na}_3\text{C}_3\text{N}_3\text{S}_3$ coordinated to the metal ions (NiCl_2) to form $\text{Ni}_3(\text{C}_3\text{N}_3\text{S}_3)_2$ coordi-

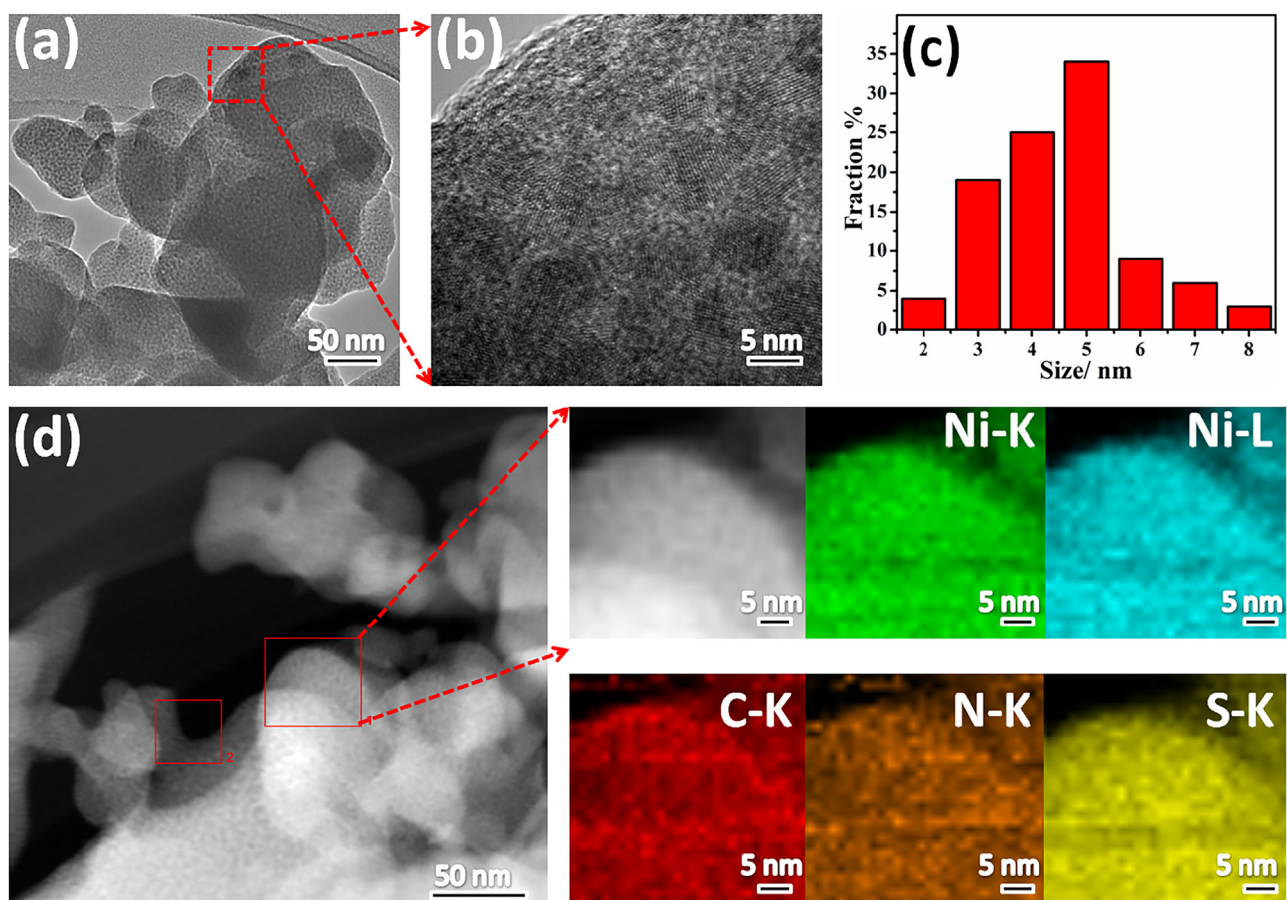


Fig. 1. (a) TEM and (b) HRTEM images of $\text{Ni}_3(\text{TMT})_2$. (c) The size distribution of nanoparticles in $\text{Ni}_3(\text{TMT})_2$. (d) The STEM image of the $\text{Ni}_3(\text{TMT})_2$ with elemental mapping images of Ni-K, Ni-L, C-K, N-K and S-K.

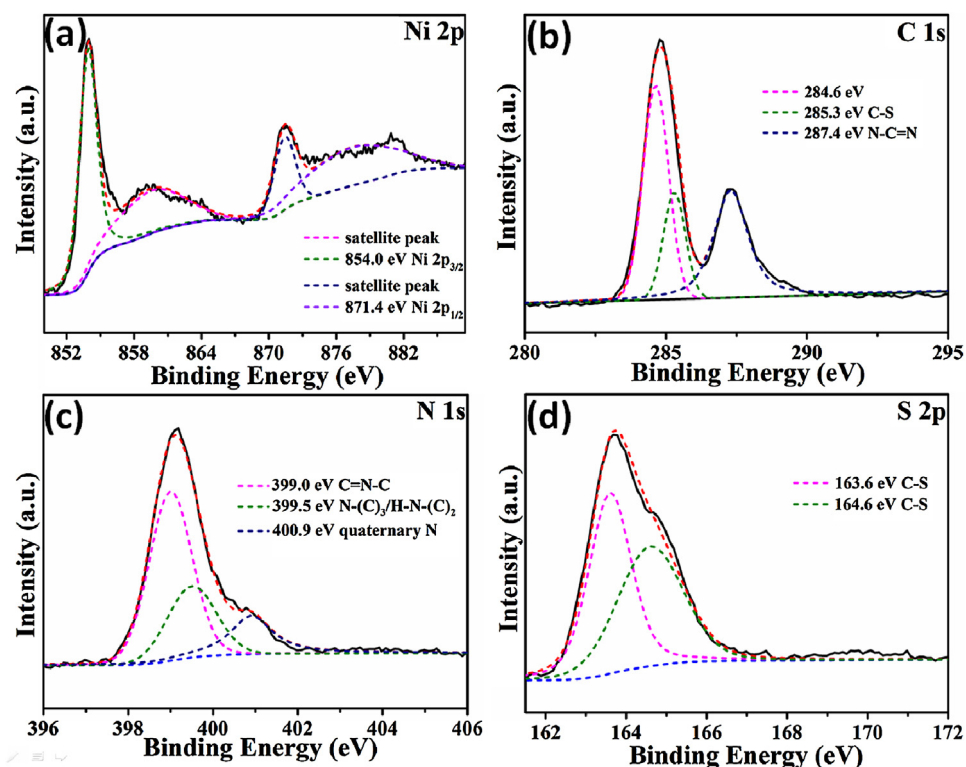


Fig. 2. High-resolution XPS spectra of $\text{Ni}_3(\text{TMT})_2$: (a) Ni 2p, (b) C 1s, (c) N 1s, and (d) S 2p.

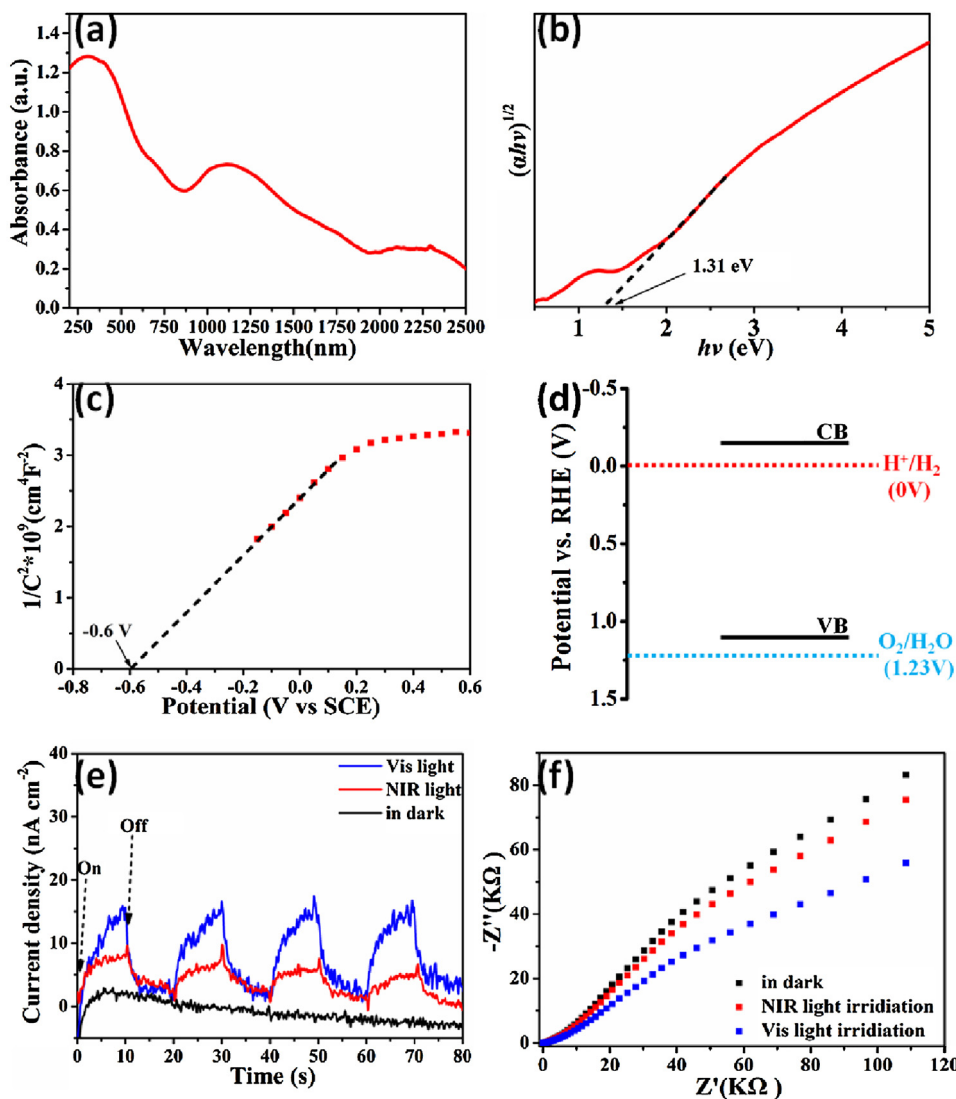


Fig. 3. (a) UV-vis-NIR diffuse reflection spectrum of as-prepared $\text{Ni}_3(\text{TMT})_2$. (b) A plot transformed according to the Kubelka-Munk function versus energy of light. (c) Mott-Schottky plot and (d) energy band structure diagram of $\text{Ni}_3(\text{TMT})_2$. (e) The photocurrent responses and (f) EIS (at open circuit potential) of $\text{Ni}_3(\text{TMT})_2$ in 0.5 M Na_2SO_4 electrolyte under Vis and NIR light as well as under dark condition as blank sample.

nation polymer. Through EDX elemental microanalysis of obtained $\text{Ni}_3(\text{C}_3\text{N}_3\text{S}_3)_2$ (Fig. S1), the molar ratio of C, N, S and Ni element is 1: 0.91: 1.13: 0.46, which testifies that the synthesized product is $\text{Ni}_3(\text{C}_3\text{N}_3\text{S}_3)_2$ and can be denoted as $\text{Ni}_3(\text{TMT})_2$ where TMT is 2,4,6-trimercaptotriazine anion.

The XRD of $\text{Ni}_3(\text{TMT})_2$ was presented (Fig.S2), which showed three broadened Bragg diffraction peaks at around 16.8° , 32.5° and 48.9° , respectively, indicating the resulting solid is an amorphous material. And the irregular bulk characteristics of $\text{Ni}_3(\text{TMT})_2$ (inset of Fig.S2) was just demonstrated by SEM. The morphology of $\text{Ni}_3(\text{TMT})_2$ was also investigated by TEM as shown in Fig. 1. In Fig. 1a, it is found that $\text{Ni}_3(\text{TMT})_2$ exhibits layered thin sheet. It is noteworthy that there are a number of quasi nanoparticles on the surface of $\text{Ni}_3(\text{TMT})_2$. Further magnification observation in Fig. 1b, it can be seen that these nanoparticles have different size with distinct lattice fringes, which may be responsible for generated NiS_x in bonding process of Ni(II) and S-bonds of TMT. The diameters of nanoparticles are in the range of 2–8 nm with an average of diameter 5 nm (Fig. 1c). The scanning transmission electron microscope (STEM) and the corresponding elemental mapping images were recorded in Fig. 1d. The result reveals that Ni, C, N and S are

detected and homogeneously distributed over the entire structure, which gives a solid evidence of the formed $\text{Ni}_3(\text{TMT})_2$.

To determine the composition and chemical states of elements, the XPS of as-prepared $\text{Ni}_3(\text{TMT})_2$ was carried out. The survey-scan XPS spectrum discloses that there are elements of Ni, C, N and S in the $\text{Ni}_3(\text{TMT})_2$ (Fig.S3). Fig. 2a exhibits the high-resolution XPS spectrum of Ni 2p. Clearly, two peaks observed at 871.4 eV and 854.0 eV with two satellite peaks around 877.5 eV and 860.5 eV correspond to the Ni 2p peaks in the chemical state of Ni (II) [18–20]. The high-resolved C 1 s XPS spectrum (Fig. 2b) can be deconvoluted into three peaks at 284.6, 285.3 and 287.4, which represent C 1 s states in C=C/C=C, C-S and N=C=N bonds, respectively [21,22]. The N 1 s spectrum (Fig. 2c) displays three peaks at 399.0, 399.5 and 400.9 eV, which can be ascribed to C=N–C, the tertiary N bonded to carbon atoms in the form of N-(C)₃ or H–N–(C)₂ and quaternary N bonded to three carbon atoms in the aromatic cycles, respectively [23,24]. In the high resolution S 2p XPS spectrum of $\text{Ni}_3(\text{TMT})_2$, two peaks at 163.6 and 164.6 eV are shown in Fig. 2d, which corresponds to the 2p_{3/2} and 2p_{1/2} positions of the –C=S– covalent bond [25]. Fig.S4 shows the FT-IR spectra of comparable samples. As discussed previously, four major peaks at 1630, 1458, 1211 and 857 cm⁻¹ in the FT-IR spectrum of 2, 4, 6-trimercaptotriazine trisodium salt

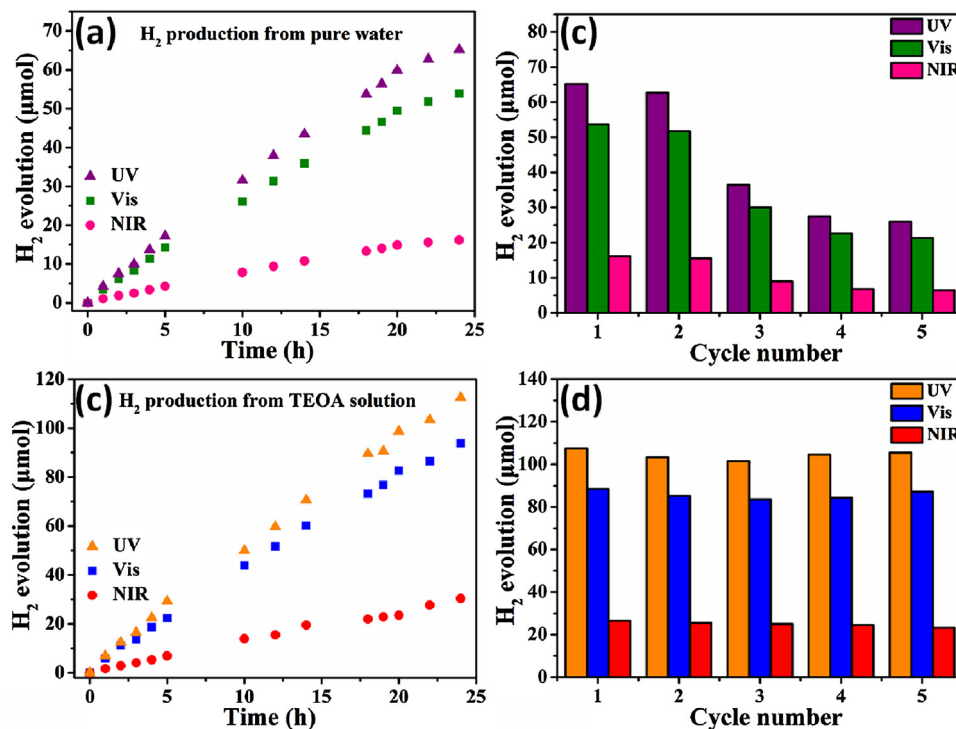


Fig. 4. (a) Time courses of photocatalytic H₂ generation and (b) the photocatalytic stability over Ni₃(TMT)₂ from pure water under UV, Vis and NIR irradiation. (c) Time courses of photocatalytic H₂ evolution and (d) the photocatalytic stability over the Ni₃(TMT)₂ in the present of TEOA (2.5 vol.%) solution under UV, Vis and NIR irradiation.

(Na₃TMT) are attributed to the characteristic of the aromatic trithiol form of TMT ring system. Compared with Na₃TMT, it is observed that the four characteristic bands of Ni₃(TMT)₂ in the FT-IR spectrum all shift toward positive, demonstrating that the coordination polymer has been formed, which is consistent with the pioneering literature [26].

The light absorption properties of Ni₃(TMT)₂ was characterized by the UV-vis-NIR diffuse reflectance spectroscopy (DRS) in Fig. 3a. The DRS absorption spectrum reveals that the Ni₃(TMT)₂ exhibited extensive optical absorption in the solar region of 200–2500 nm, which apparently tailed out till NIR range without extinction. Thus, it is inferred that Ni₃(TMT)₂ may be a potential NIR-response photocatalyst. Through calculating the band gap energy based on the formula $(\alpha h\nu)^{1/2} \propto h\nu - E_g$, where α , h , ν and E_g were absorption coefficient, Planck constant, light frequency and band gap energy, respectively. The E_g of Ni₃(TMT)₂ was calculated to be 1.31 eV (Fig. 3b), implying Ni₃(TMT)₂ can be activated by NIR light irradiation. To better understand energy band structure of the Ni₃(TMT)₂, the Mott-Schottky (MS) equation was further applied for studying the flat band potential of Ni₃(TMT)₂. In Fig. 3c, it is obtained that the Ni₃(TMT)₂ was a typical *n*-type semiconductor according to a positive slope [27]. Based on the MS plot, the flat band potential is calculated to be −0.6 V vs. SCE, and equals to −0.36 vs. NHE. It is reported that the flat band potential is 0.1–0.3 eV lower than the conduction band in the *n*-type semiconductor [28]. Consequently, the CB for Ni₃(TMT)₂ is estimated to be −0.15 V vs. RHE. And the valence band (VB) position is calculated as 1.16 V vs. RHE based on its band gap. To compare with the potentials for water reduction and oxidation, Fig. 3d displays the energy level diagram of Ni₃(TMT)₂. Obviously, the CB and VB are −0.15 eV and 1.16 eV, respectively. The CB level is more negative than the standard reduction potential of a proton, while the VB potential is lower than the standard oxidation potential of water, which demonstrated the reduction reaction of water may be thermodynamically carried out, while water oxidation may not be feasible for Ni₃(TMT)₂. As can be seen in Fig. 3e and f, both transient photocurrent response and

Nyquist plots of EIS for Ni₃(TMT)₂ were carried out under Vis, NIR light irradiation and darkness. The Ni₃(TMT)₂ electrode illustrates 15.7 nA cm^{−2} under Vis light irradiation, and 9.3 nA cm^{−2} under NIR light irradiation but no response in the dark (Fig. 3e). The different current densities mainly resulted from the different optical absorptions and optical densities, which were Vis light for 31.7 mW cm^{−2} and NIR light for 10.8 mW cm^{−2}. Also, the arc radius on EIS Nyquist plot under Vis light illumination is smaller than that of under the NIR light illumination and in the dark (Fig. 3f). The above results illustrate that Ni₃(TMT)₂ can be induced electron-hole pairs under the Vis and NIR light irradiation, which is the primary requirement for Vis and NIR light photocatalytic activity of Ni₃(TMT)₂.

The photocatalytic activities of as-prepared Ni₃(TMT)₂ were tested by H₂ evolution in pure water under different wavelength ranges without any sacrificial agents or cocatalysts (Fig. 4a). As might be expected, H₂ was constantly generated but no O₂ evolution over the Ni₃(TMT)₂ in photocatalytic process. And the amounts of H₂ production are 65.3 μmol, 53.9 μmol and 16.3 μmol corresponding to UV ($\lambda < 400$ nm), Vis ($400 \leq \lambda \leq 760$ nm) and NIR ($\lambda > 760$ nm) irradiation after 24 h, respectively. However, after five successive cycling runs, the amounts of H₂ generated obviously declined (Fig. 4b). It is worthwhile mentioning that when the TEOA as a sacrificial agent was injected into the reaction system (Fig. 4c), the H₂ evolution of Ni₃(TMT)₂ increased from 65.3 μmol to 112.6 μmol, 53.9 μmol to 93.3 μmol and 16.3 μmol to 30.1 μmol corresponding to under UV, Vis and NIR irradiation after 24 h. Moreover, the photostability of Ni₃(TMT)₂ was effectively improved with the assistance of TEOA. Significantly, no apparent activities decrease of Ni₃(TMT)₂ could be obtained after five cycling times (Fig. 4d).

In order to investigate the difference before and after photocatalytic reactions with or without a sacrificial agent, the XPS spectra of corresponding S 2p and N 1s of Ni₃(TMT)₂ with different samples were presented in Fig. 5. Obviously, compared with the fresh sample (Fig. 5a and b), S^{2−} and N^{3−} in the Ni₃(TMT)₂ could be oxidized by photo-induced holes (h^+) to generate sulfite (167.4 eV) and

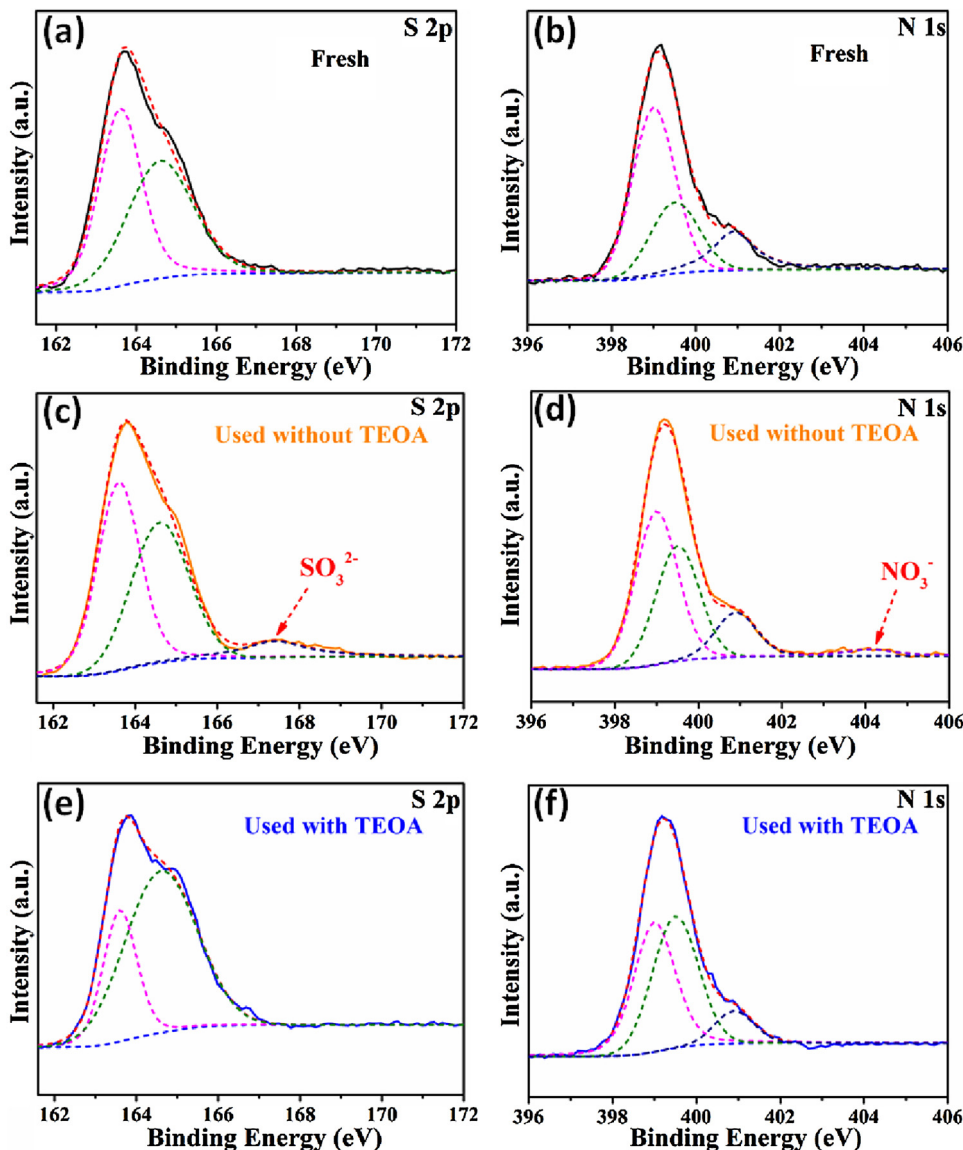


Fig. 5. High-resolution XPS spectra of the $\text{Ni}_3(\text{TMT})_2$: S 2p and N 1s spectra of fresh sample (a, b), after photocatalytic reaction for 120 h under visible light irradiation with TEOA (c, d) or without TEOA (e, f).

nitrite (404.1 eV) after a reaction time due to the photo-corrosion during the half reaction (Fig. 5c and d) [29]. And the use of TEOA as a sacrificial agent added into photocatalytic reaction could have a positive effect on the photocatalytic activity and stability of the $\text{Ni}_3(\text{TMT})_2$ for H_2 evolution. Through the XPS spectra of S 2p and N 1s (Fig. 5e and f), it can be seen no sulfite and nitrite derived from the photo-corrosion of $\text{Ni}_3(\text{TMT})_2$ when the photocatalytic activities of $\text{Ni}_3(\text{TMT})_2$ sample was tested, which is matchable well with the above experimental results.

The above results reveal that the formation of $\text{Ni}_3(\text{TMT})_2$ and its photocatalytic properties under UV, Vis, and NIR irradiation. And the mechanism for the photocatalytic H_2 production is proposed in Fig. 6. The $\text{Ni}_3(\text{TMT})_2$ coordination polymer, as a board spectrum-active photocatalyst, is absorbed by the light with larger energy than its band gap, and photo-induced electrons and holes were simultaneously generated by excitation, which induced photogenerated electrons from VB to CB, leaving holes in the VB, then migrated to the surface of the bulk. Generally, the electrons reduced protons to generate H_2 while the photogenerated holes were accumulated in the bulk of the catalyst without a sacrificial agent,

leading to the self-oxidation of the $\text{Ni}_3(\text{TMT})_2$ as above mentioned the XPS results. When TEOA was added into the photocatalytic reaction, the photogenerated holes combined with TEOA to form TEOA⁺ instead of self-oxidation of $\text{Ni}_3(\text{TMT})_2$ for effectively enhancing the stability of the photocatalyst, and generated H_2 production was also obviously improved under UV, Vis and NIR light irradiation.

4. Conclusion

We have successfully synthesized a novel $\text{Ni}_3(\text{TMT})_2$ coordination polymer by a facile wet-chemical rout for the first time. Specifically, the as-prepared $\text{Ni}_3(\text{TMT})_2$ possessed UV–NIR broad spectrum absorption and can be acted as a board spectrum-driven photocatalyst for water splitting into hydrogen. As expected, the H_2 production performance from pure water over $\text{Ni}_3(\text{TMT})_2$ was realized through from UV ($\lambda < 400 \text{ nm}$) to Vis ($400 \leq \lambda \leq 760 \text{ nm}$) and NIR ($\lambda > 760 \text{ nm}$) without any sacrificial agents or cocatalysts, and the amounts of H_2 production are 65.3, 53.9 and 16.3 μmol corresponding to UV, Vis and NIR irra-

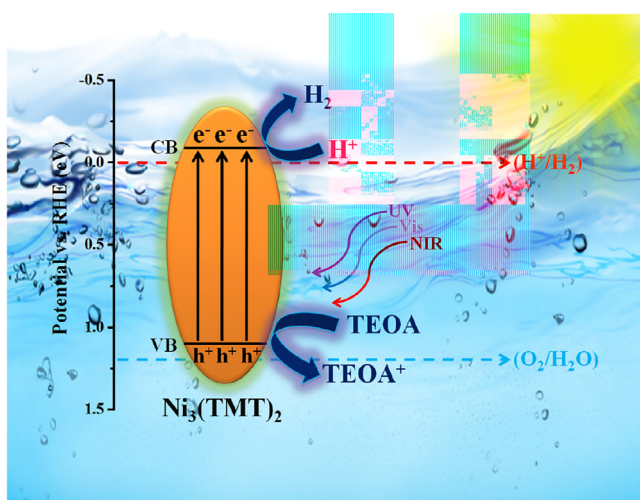


Fig. 6. The proposed charge separation process of $\text{Ni}_3(\text{TMT})_2$ under solar light irradiation.

diation after 24 h, respectively. Significantly, the efficiency of H_2 production and the stability over the $\text{Ni}_3(\text{TMT})_2$ could be improved with the assistance of TEOA. And the average H_2 evolution efficiencies on $\text{Ni}_3(\text{TMT})_2$ were efficaciously increased by around 2-fold with the H_2 production value of 112.6, 93.3 and 30.1 μmol for 24 h under the UV, Vis and NIR light exposure, respectively. Although the H_2 -producing activity of $\text{Ni}_3(\text{TMT})_2$ coordination polymer just displayed from the half-reaction of water splitting, the results facilitate the increasing attention of narrow band gap non-noble metal coordination polymer treated as board-spectrum driven photocatalysts for expanding the utilization of solar light.

Acknowledgements

This work is supported by Collaborative Innovation Center of Suzhou Nano Science and Technology, the National Natural Science Foundation of China (51422207, 51132006, 51572179, 21471106, 21501126), the Specialized Research Fund for the Doctoral Program of Higher Education (20123201110018) and a project funded by the Priority Academic Program Development of Jiangsu Higher Education Institutions (PAPD).

Appendix A. Supplementary data

Supplementary data associated with this article can be found, in the online version, at <http://dx.doi.org/10.1016/j.apcatb.2017.03.062>.

References

- [1] Q. Zhang, E. Uchaker, S.L. Candelaria, G. Cao, Chem. Soc. Rev. 42 (2013) 3127–3171.
- [2] A. Fujishima, K. Honda, Nature 238 (1972) 37–38.
- [3] X. Wang, Z. Li, J. Shi, Y. Yu, Chem. Rev. 114 (2014) 9346–9384.
- [4] Y.M. He, Y. Wang, L.H. Zhang, B.T. Teng, M.H. Fan, Appl. Catal. B: Environ. 168 (2015) 1–8.
- [5] R. Lamba, A. Umar, S.K. Mehta, S.K. Kansal, J. Alloys Compd. 653 (2015) 327–333.
- [6] Y. Li, M.H. Cao, L.Y. Feng, Langmuir 25 (2009) 1705–1712.
- [7] S. Kohtani, M. Koshiko, A. Kudo, K. Tokumura, Y. Ishigaki, A. Toriba, K. Hayakawa, R. Nakagaki, Appl. Catal. B: Environ. 46 (2003) 573–586.
- [8] H.Q. Li, X. Wang, J.Q. Xu, Q. Zhang, Y. Bando, D. Golberg, Y. Ma, T.Y. Zhai, Adv. Mater. 25 (2013) 3017–3037.
- [9] W. Qin, D. Zhang, D. Zhao, L. Wang, K. Zheng, Chem. Commun. 46 (2010) 2304–2306.
- [10] H. Tong, S.X. Quyang, Y.P. Bi, N. Umezawa, M. Oshikiri, J.H. Ye, Adv. Mater. 43 (2012) 229.
- [11] Z.J. Zhang, W.Z. Wang, Dalton Trans. 42 (2013) 12072–12074.
- [12] C. Li, F. Wang, J. Zhu, J.C. Yu, Appl. Catal. B: Environ. 100 (2010) 433–439.
- [13] Z.K. Zheng, T. Tachikawa, T. Majima, J. Am. Chem. Soc. 136 (2014) 6870–6873.
- [14] J. Tian, Y.H. Sang, G.W. Wei, H.D. Jiang, X.N. Mu, H. Liu, Adv. Mater. 25 (2013) 5075–5080.
- [15] Y.H. Sang, Z.H. Zhao, M.W. Zhao, P. Hao, Y.H. Leng, H. Liu, Adv. Mater. 27 (2015) 363–369.
- [16] H.Q. Zhuang, L.F. Yang, J. Xu, F.Y. Li, Z.Z. Zhang, H.X. Lin, J.L. Long, X.X. Wang, Sci. Rep. 5 (2015) 16947.
- [17] S.Y. Zhao, C.X. Li, J. Liu, N.Y. Liu, S. Qiao, Y.Z. Han, H. Huang, Y. Liu, Z.H. Kang, Carbon 92 (2015) 64–73.
- [18] F. Loglio, M. Innocenti, A. Jarek, S. Caporali, I. Pasquini, M.L. Foresti, J. Electroanal. Chem. 638 (2010) 15–20.
- [19] A.N. Buckley, R. Woods, J. Appl. Electrochem. 21 (1991) 575–582.
- [20] H.W. Nesbitt, D. Legrand, G.M. Bancroft, Phys. Chem. Miner. 27 (2000) 357–366.
- [21] S. Liu, J. Tian, L. Wang, Y. Zhang, X. Qin, Y. Luo, A.M. Asiri, A.O. Al-Youbi, X. Sun, Adv. Mater. 24 (2012) 2037–2041.
- [22] D. Sun, R. Ban, P.H. Zhang, G.H. Wu, J.R. Zhang, J.J. Zhu, Carbon 64 (2013) 424–434.
- [23] V.N. Khabashesku, J.L. Zimmerman, J.L. Margrave, Chem. Mater. 12 (2000) 3264–3270.
- [24] T. Komatsu, T. Nakamura, J. Mater. Chem. 11 (2001) 474–478.
- [25] J. Xu, L.F. Luo, G.R. Xiao, Z.H. Zhang, H.X. Lin, X.X. Wang, J.L. Long, ACS Catal. 4 (2014) 3302–3306.
- [26] R.S. Vishwanath, K. Sakthivel, J. Electrochem. Soc. 163 (2016) 402–409.
- [27] J. Zhang, X. Chen, K. Takanabe, K. Maeda, K. Domen, J.D. Epping, X. Fu, M. Antonietti, X. Wang, Angew. Chem. Int. Ed. 49 (2010) 441–444.
- [28] H. Kim, P. Borse, W. Choi, J. Lee, Angew. Chem. Int. Ed. 44 (2005) 4585–4589.
- [29] J.F. Moulder, W.F. Stickle, P.E. Sobol, K.D. Bomben, Physical Electronic, Inc. USA, 1992.